mater.scichina.com link.springer.com

Sci China Mater 2025, 68(12): 4534–4545
https://doi.org/10.1007/s40843-025-3580-0

Highly robust and fatigue-resistant organic hydrogel composite elastomer fibers with multi-sensing capabilities

Jiaxin Shen[1], Tao Feng[1], Chen Li[1], Shisheng Hou[1], Kuibo Yin[1], Hengchang Bi[2,3*] and Litao Sun[1*]

ABSTRACT **Converting hydrogels into one-dimensional (1D) fiber structures and integrating them into textiles offers a promising approach for the development of smart wearable devices. However, under repeated deformations, the fracture of low-energy amorphous crosslinking structure in the hydrogel leads to fatigue and hysteresis. This severely impairs the mechanical properties of hydrogel fibers and limits their potential applications. In this study, a novel strategy for fabricating composite hydrogel smart fibers featuring exceptional mechanical robustness and multisensory capabilities is proposed. By integrating an Ecoflex elastomer backbone into the organic hydrogel, the fatigue resistance is enhanced and hysteresis is eliminated, and no significant degradation of mechanical properties is observed after 10,000 cycles of 200% strain loading and unloading. The strain sensor based on this fiber has high sensitivity (gauge factor ~3.0), fast response (140 ms)/recovery time (130 ms), and excellent repeatability (10,000 cycles at 70% strain). Moreover, the organic hydrogel/Ecoflex fiber (OHEF) exhibits remarkable resistance to dehydration and freezing. Smart textiles based on OHEF can detect diverse external stimuli, including deformation, temperature, proximity, pressure, and can perform passive sensing. The successful development of this fiber represents significant progress in applying hydrogels to wearable devices. Its multisensory properties highlight the great potential of OHEF for wearable electronics applications.**

Keywords: smart fiber, hydrogel, flexible electronics, triboelectric nanogenerator

INTRODUCTION

Textiles function as the interface between the human body and the external environment [1–4]. When compared with film-based electronic skins [5–8], textile-based electronics endow wearable electronics with superior flexibility, breathability, and comfort [9–12]. As a result, they open up new avenues for enhancing the performance of wearable devices. The integration of sensory functions into textiles is expected to fundamentally revolutionize the way humans interact with electronic devices. By sensing the external environment and human physiological signals, textiles can be endowed with intelligent feedback capabilities. This promotes the further development of smart wearable devices [13–16]. Fibers are the basic components of textiles. For diverse application scenarios, based on material properties and structural design, researchers have developed a series of smart fibers with functions such as response, detection, feedback, and regulation. This enables the sensing [17–20], displaying [21–23], and powering smart textiles [24,25]. Conductive smart fibers are usually fabricated by embedding rigid substances or nanomaterials into elastomers [26–30]. However, this approach gives rise to inevitable problems, such as insufficient robustness and biocompatibility. These problems severely restrict the wide application of smart fibers [31,32].

Hydrogels are crucial materials for flexible ionic electronics due to their intrinsic ionic conductivity [33–38]. Hydrogels, with their conductive flexibility and biocompatibility, are applied in a diverse array of modern technologies [39,40], including tissue engineering [41], drug delivery [42], biomedical devices [43], microfluidics [44], optics [45], stretchable and bio-integrated electronics [46], and soft robotics [47]. Especially, cellulose-based hydrogels [48,49] have great potential for application in emerging intelligent sensors [50–52]. Therefore, hydrogel fibers that are robust, biocompatible, mechanically strong, and highly ionically conductive hold the potential to be woven into the desired intelligent textiles [53]. However, during repeated deformations, the fracture of the low-energy amorphous crosslinking structure in the hydrogel leads to fatigue and hysteresis, thereby weakening the mechanical properties. This significantly restricts the application potential of hydrogel fibers [54]. Therefore, improving these two aspects is a key problem that urgently requires exploration and solution. If these problems can be resolved, hydrogel-based fibers might play a role in future smart devices and equipment.

In this study, we present a bicontinuous-structured hydrogel fiber featuring an elastomer backbone. This fiber demonstrates remarkable fatigue resistance and robustness, allowing it to promptly and precisely respond to a wide range of physiological and external signals. The fiber was fabricated through embedding an organic hydrogel into a porous Ecoflex matrix, which was prepared via the sacrificial-template method. Due to the support and protection provided by the elastic Ecoflex backbone, the fibers display excellent mechanical robustness and conductive stability. Additionally, they resist drying and freezing. Moreover, due to the inherent ionic conductivity and unique bicontinuous structure of the organic hydrogel, the fiber can

[1] SEU-FEI Nano-Pico Center, Key Laboratory of MEMS of Ministry of Education, Collaborative Innovation Center for Micro/Nano Fabrication, Device and System, Southeast University, Nanjing 210096, China
[2] Chongqing Key Laboratory of Precision Optics, Chongqing Institute of East China Normal University, Chongqing 401120, China
[3] In Situ Devices Center, School of Integrated Circuits, East China Normal University, Shanghai 200241, China
* Corresponding author (email: hcbi@cee.ecnu.edu.cn; slt@seu.edu.cn)

precisely and promptly respond to diverse external stimuli, such as deformation, temperature, pressure, proximity, and passive sensing facilitated by nano-friction generators. The successful fabrication of this strong and robust hydrogel-elastomer composite fiber will propel substantial progress in the functionalization and application of highly robust hydrogel fibers. Additionally, the development of its related smart textiles will revolutionize the human-machine interface, providing excellent flexibility and comfort, and bringing great convenience to humans' smart life.

EXPERIMENTAL SECTION

Materials

Chitosan (CHI) with a viscosity of 50–800 mPa s was purchased from Sinopharm Chemical Reagent Co., Ltd., China. Acrylamide (AAM), glycerol, and $Al(NO_3)_3{\cdot}9H_2O$ were purchased from Shanghai Aladdin Biochemical Technology Co., Ltd., China. *N*,*N*′-methylene bisacrylamide, benzophenone, and NaCl were supplied by Shanghai Macklin Biochemical Co., Ltd., China. Ecoflex 00–30 (Smooth-on) was purchased from Smooth-On Co., Ltd. Irgacure 2959 was obtained from BASF Co., Ltd. Deionized (DI) water was used in all the experiments. All the reagents were used without further purification.

Preparation of organic hydrogel/Ecoflex fiber (OHEF)

The organic hydrogel (o-hydrogel) was synthesized via the one-pot method as shown in Fig. S1. Its rheological properties are shown in Fig. S2.

The preparation of porous Ecoflex was carried out as follows: Ecoflex is divided into liquid A and liquid B, where liquid A is a siloxane chain polymer and liquid B is a crosslinking agent. Benzophenone (0.4 wt%) was added to liquid A of Ecoflex, and the mixture was stirred at 60 °C for 30 min and then cooled. Next, 0.5 wt% retarder was added to liquid B of Ecoflex. Liquid A and liquid B were mixed in a 1:1 mass ratio. Subsequently, NaCl particles with twice the mass of Ecoflex were added to the Ecoflex, and the resulting mixture was placed in a fine-tube template. After curing at 60 °C for 120 min, the NaCl template was washed away with water, and the mixture was dried to obtain porous Ecoflex.

The preparation of OHEF was performed as follows: an o-hydrogel precursor solution was adsorbed into the porous Ecoflex via vacuum-assisted method, and then the sample was exposed to UV light at 365 nm for 2 h to polymerize the o-hydrogel and form strong interfacial bonds. Subsequent to demolding, an additional layer of Ecoflex was attached to the exterior and cured to encapsulate the porous Ecoflex and the inner o-hydrogel, thus obtaining the OHEF.

The difficulty of this process lies in the removal of the NaCl template and the adsorption of the organic hydrogel solution. The specific implementation plan is shown in Fig. S3.

Characterization

For cross-sectional observation, OHEF samples were observed after 48 h of lyophilization. The samples were cryo-fractured in liquid nitrogen to obtain clean cross-sections. The morphology was observed by scanning electron microscopy (SEM, Helios 5 CX Dual Beam, Thermo Scientific) at an acceleration voltage of 10 kV. All samples were sputtered with gold of 3–5 nm thickness before imaging. Thermal transition properties were measured by a differential scanning calorimeter (DSC, NETZSCH STA 2500) at a heating/cooling rate of 10 °C/min from room temperature to −100 °C. The mechanical properties were tested at room temperature using a dynamometer (Mark-10) with a 10 N load cell. The electromechanical behavior of the samples was measured using a digital source meter (KEITHLEY 2450). The electric outputs of the OHEF-TENG were measured by a Keithley 6514 electrometer.

Ethical statement

The authors confirmed that there was no need to obtain Institutional Review Board approval because the volunteer conducted the study using wearable sensors and simple contact measurement devices without any physical modifications or invasive measurements on the human bodies. In addition, the volunteer was one of the authors of the testing of the sensor devices. The requirements and possible risks of these tests had been fully informed before the tests. The volunteers gave written consent before participating in the experiments.

RESULTS AND DISCUSSION

Design and preparation of OHEF

OHEF was fabricated via a process involving sacrificial templating, vacuum-assisted adsorption, UV cross-linking, and Ecoflex encapsulation. Ecoflex, an elastomeric material characterized by good flexibility and processability, plays crucial roles in backbone support and encapsulation within this system. Firstly, a porous Ecoflex backbone was prepared by the sacrificial template method. Solid template particles (sodium chloride) were homogeneously mixed with Ecoflex at a specific mass ratio and then placed into a fine tube. Fig. S4 shows the effect of different ratios of NaCl template to Ecoflex on OHEF. In this work, the mass ratio of NaCl to Ecoflex was determined to be 2:1. After Ecoflex was cured, the template was removed with water to yield a porous Ecoflex backbone. Subsequently, the organic hydrogel pre-gel solution was adsorbed into the porous Ecoflex fibers via vacuum-assisted method. After the o-hydrogel was cross-linked by UV, the entire system was demolded from the fine tube. Finally, a layer of Ecoflex was externally wrapped to serve as an encapsulation layer, thereby obtaining OHEF. The Ecoflex encapsulation layer not only safeguards the inner o-hydrogel and porous Ecoflex against external environmental factors but also enhances the mechanical properties and stability of the entire OHEF structure. The entire fabrication process is depicted in Fig. 1a.

The OHEF fabricated by this method displays remarkable mechanical robustness, characterized by fatigue resistance and the absence of hysteresis. This can be ascribed to the supporting and encapsulating effects of the elastomeric skeleton. When the fiber is stretched, the internal o-hydrogel deforms and recovers in synchrony with the elastomeric skeleton, as shown in Fig. 1b. The stable binding of the o-hydrogel to Ecoflex within the porous Ecoflex skeleton is of crucial importance. Benzophenone, functioning as an oxygen barrier and a UV-assisted grafting agent, promotes the effective binding of the o-hydrogel to Ecoflex (Fig. 1c, Figs S5 and S6). In terms of appearance, the physical photograph of OHEF shown in Fig. 1d clearly reveals its uniform texture. Owing to the template-based preparation method, the fibers exhibit good diameter consistency, which ensures their performance stability in practical applications.

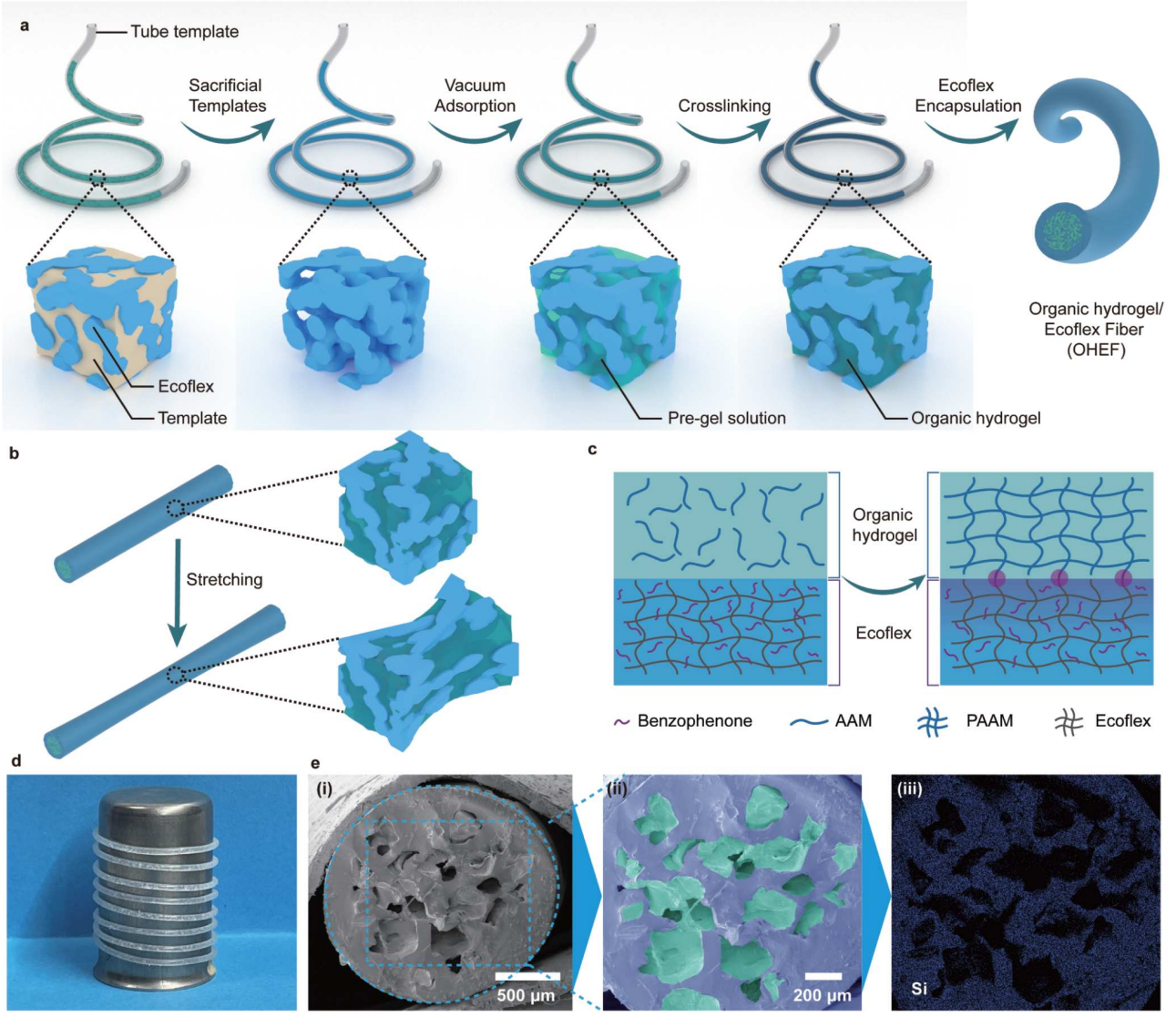

Figure 1 Preparation and demonstration of OHEF. (a) Schematic illustration of the preparation steps of OHEF. (b) Schematic representation of the deformation of the internal bicontinuous structure during OHEF stretching. (c) Schematic of the interfacial bonding between o-hydrogel and Ecoflex. (d) Photograph of OHEF. (e) SEM images (i, ii) and EDS mapping of OHEF (iii).

Subsequently, the cross-section of the fiber was observed using a scanning electron microscope. As depicted in Fig. 1e(i), the o-hydrogel and porous Ecoflex were inter-embedded. The o-hydrogel was clearly visible, with a tight interfacial bond and no visible voids, which serves as strong evidence of the good compatibility and combination between the two materials. To facilitate observation, the o-hydrogel and Ecoflex were colored differently in Fig. 1e(ii). The green part corresponded to the polymer network formed by freeze-drying the o-hydrogel, and the blue part was Ecoflex. The energy dispersive spectroscopy (EDS) elemental mapping image also revealed this structure (Fig. 1e(iii)).

Anti-fatigue of OHEF

Most hydrogel fibers reported thus far inevitably experience creep following repeated stretching due to the material's inherent fatigue, consequently affecting their performance and service life (Fig. 2a). This has undoubtedly emerged as a bottleneck restricting the application of hydrogel fibers in numerous fields where material durability and stability are crucial. In this study, a porous Ecoflex elastomer was embedded in the o-hydrogel as a backbone. The Ecoflex elastomer can effectively mitigate the material fatigue problem, thereby enhancing the fiber's mechanical stability and conferring resistance to fatigue and creep. The reinforcement of the o-hydrogel by the porous Ecoflex is manifested in two aspects: the supporting effect and the encapsulating effect. Regarding the support aspect, the porous Ecoflex elastomer constructs a solid physical support framework within the o-hydrogel owing to its stable and robust three-dimensional network structure. When OHEF is subjected to an external tensile force, in the axial direction, the skeleton exerts a tensile force on the o-hydrogel, causing the o-hydrogel to elongate and deform axially. Simultaneously, in the radial direction, the skeleton exerts a compressive effect on the o-hydrogel, leading to the o-hydrogel's radial contraction. During this process, the o-hydrogel closely adheres to the skeleton's deformation pattern. This synergistic deformation mechanism remarkably improves the structural stability and consistency of

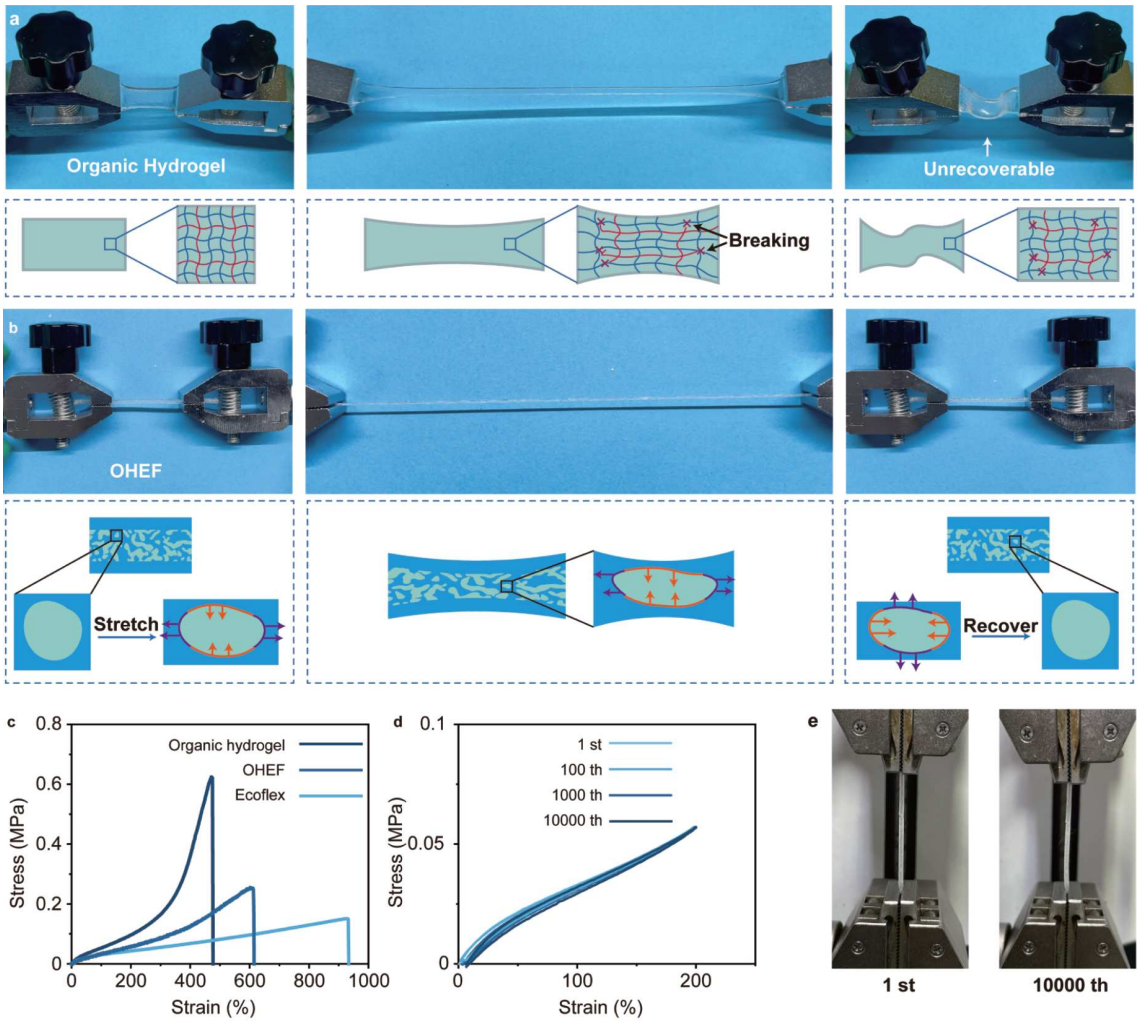

Figure 2 Mechanical properties of OHEF. Stretching and recovery behaviors of (a) o-hydrogel and (b) OHEF. (c) Stress-strain curves of o-hydrogel, Ecoflex, and OHEF. (d) Cyclic loading and unloading curves of OHEF. (e) Initial photograph of OHEF and photo after 10,000 cycles at 200% strain.

the overall mechanical response of OHEF under stress, effectively preventing structural damage and performance degradation induced by stress concentration within the o-hydrogel. Regarding encapsulation, the pore structure of the porous Ecoflex can exert a certain wrapping and restraining effect on the o-hydrogel, restricting the excessive slip and rearrangement of the o-hydrogel's molecular chains during stress application. This further enhances the composite fiber's fatigue and creep resistance. These two effects do not exist independently but interact synergistically, thereby jointly enhancing the comprehensive mechanical properties of OHEF (Fig. 2b).

Subsequently, to thoroughly investigate the mechanical behaviors of the constituent materials and composite fibers, the stress-strain properties of Ecoflex, the o-hydrogel, and OHEF were measured separately (Fig. 2c). Ecoflex elastomer displays a tensile strength of 0.62 MPa, the highest among the three. Such excellent mechanical properties endow it with an inherent advantage as a backbone material in the OHEF system. In contrast, due to their high water content, o-hydrogels contain a large number of freely movable water molecules, endowing them with strong deformability. Under low stress, the o-hydrogel can deform significantly. However, when the external force is removed, due to the mobility of water molecules and the weak interactions between o-hydrogel molecular chains, its recovery to the initial state is poor, with obvious residual deformation. However, the situation changed significantly when Ecoflex was ingeniously introduced into the o-hydrogel system as a supporting skeleton. The o-hydrogel is tightly bonded to the Ecoflex skeleton via physical entanglement, hydrogen bonding, and other interactions. This enables the o-hydrogel to be supported and restrained by the Ecoflex skeleton when subjected to force, effectively enhancing its mechanical properties and significantly improving its resistance to deformation and recovery to the original state. To further assess the performance of OHEF under cyclic loading in practical applications, continuous loading-unloading experiments were designed in this study. The experiment was conducted at a high strain of 200% and a strain rate of 50% per second. After 10,000 loading cycles, the stress-strain curves of OHEF were analyzed in detail, and the results were promising. As depicted in Fig. 2d, the stress-strain curve of OHEF exhibits negligible hysteresis throughout the cycle, indicating minimal energy loss during repeated loading and unloading. Simultaneously, the tensile-strength monitoring data indicate that the tensile strength has scarcely decreased and

remains above 98% of the initial value, fully demonstrating the excellent fatigue resistance of OHEF. This excellent performance indicates that the incorporation of the Ecoflex backbone effectively enhances the mechanical properties of OHEF, effectively suppressing the hysteresis and fatigue issues typical of traditional hydrogel fibers (Table S1). In Fig. 2e, by comparing the initial state of OHEF under 200% strain with the photo after 10,000 cycles, it can be clearly seen that the fiber's appearance has not changed significantly. This further validates the structural stability and mechanical-property reliability of OHEF during cyclic loading and provides a solid experimental foundation for its extensive application in practical engineering.

Anti-dehydration and anti-freezing of OHEF

Long-term stability represents a significant challenge in the practical applications of hydrogels and hydrogel fibers, especially when wearable devices are incorporated into textiles. Conventional hydrogels are essentially composed of polymer network interwoven with a large number of water molecules and possess a very high water content, typically up to 90% or even higher. The water in hydrogels evaporates at room temperature and pressure. As water evaporates, surface tension causes the polymer network to gradually collapse. This degradation of the microstructure significantly impacts the macroscopic performance. The hydrogel undergoes significant shape changes such as shrinkage and distortion. Its flexibility declines substantially, becoming stiff and fragile, with nearly complete loss of elastic recovery capability. Meanwhile, its electrical conductivity also drops sharply. For hydrogel fibers in wearable devices to perform functions such as sensing and signal transmission, this situation is undoubtedly detrimental. It severely restricts the application of hydrogel fibers in fields such as wearable electronics, smart textiles, and other related areas. In contrast, the introduction of a glycerol/water binary solvent into the o-hydrogel system, facilitated by the presence of glycerol molecules, alters the physicochemical properties of the solvent system. Glycerol, with its relatively high molecular weight and strong intermolecular forces, can form an extensive hydrogen-bonding network with water molecules. This leads to a significant decrease in the vapor pressure of the glycerol/water binary solvent relative to traditional single-water solvents, effectively suppressing the rate of water evaporation. Furthermore, the o-hydrogel is encapsulated in the microcavities of the porous Ecoflex, and this encapsulation synergistically contributes to the outstanding long-term stability of OHEF. The freshly prepared OHEF exhibited conductivity and high stretchability at room temperature. It could conduct electricity in a circuit, causing an LED to emit light. When stretched, the resistance of OHEF increased, leading to a reduction in the LED's brightness as the partial voltage increased (Fig. 3a). Although OHEF remained highly stretchable at −20 °C (Fig. 3b), its conductivity decreased slightly, which could be ascribed to the reduced mobility of the ions responsible for conductivity. After storing the OHEF samples under natural environmental conditions for two months and re-assessing their performance, the LEDs could emit light normally with the same brightness as in the initial state (Fig. 3c). This phenomenon intuitively indicates that the electrical performance of OHEF remains stable after extended environmental storage.

Hydrogel, o-hydrogel, and OHEF were placed in the same environment (50% humidity, 20 °C) to compare their solvent-retention capacities. Solvent retention was evaluated based on the ratio of the real-time mass to the original mass (Fig. 3d). Hydrogel lost nearly all of its water within 10 days. O-hydrogel gradually lost water during the first 30 days and retained over 90% of its initial weight after 80 days. In contrast, OHEF showed no significant mass change within 80 days. The introduction of the organic solvent glycerol and the encapsulation by Ecoflex enabled water retention, thereby stabilizing the ionic conductivity in OHEF (Fig. 3e). Consequently, OHEF sustained good electrical conductivity over an extended period. Collectively, the above experimental results clearly indicate that OHEF has the potential for long-term applications, providing a solid experimental foundation for its practical implementation in fields such as wearable devices. Moreover, the application of hydrogels at low temperatures poses a significant challenge. At low temperatures, the formation of ice crystals disrupts the polymer-network structure within the hydrogel, leading to the loss of the hydrogel's flexibility, elasticity, and functionality, and ultimately causing its failure. In contrast, the thermodynamic properties of the o-hydrogel system are significantly altered because of the hydrogen-bonding formation among glycerol, water, and the polymer network, leading to a substantial decrease in its freezing point. Therefore, the freezing resistance of hydrogel and o-hydrogel was tested using DSC. As depicted in Fig. S7, no crystallization peaks were detected in the DSC thermograms of the o-hydrogel within the temperature range of −100 to 20 °C. The o-hydrogel exhibited freezing resistance, and OHEF maintained electrical conductivity at low temperatures (Fig. 3f). These results imply that o-hydrogels have excellent low-temperature tolerance, which is vital for electronics operating in low-temperature environments. Subsequently, we investigated the dynamic stability of OHEF after extended placement and exposure to low temperatures. Initially, the freshly prepared OHEFs were subjected to continuous-strain tests. A dynamic mechanical analyzer was used to apply periodic tensile strains to the fibers at a set strain amplitude and frequency while simultaneously monitoring their electrical-resistance response in real-time. The experimental results indicate that the initial fibers displayed a stable conductive response during continuous strain (Fig. 3g). After storing the OHEF at 25 °C for 60 days and conducting the same strain-loading and unloading experiments, the resistive response was consistent with that of the initial OHEF (Fig. 3h). Moreover, after storing the initial OHEF at −20 °C for 24 h and testing the resistance response in the same way, it was identical to that of the initial fibers (Fig. 3i). In addition, OHEF also has a certain degree of high temperature tolerance (Fig. S8). Collectively, the results of the above-mentioned series of experiments fully demonstrate that OHEF can exhibit excellent static and dynamic stability after both long-term storage at room temperature and short-term exposure to low temperatures. This provides a strong performance guarantee for its extensive applications in complex environmental conditions.

Response and applications of OHEF strain sensor

Most hydrogels reported hitherto exhibit significant hysteresis in their resistive responses. This characteristic makes hydrogel-based strain sensors unsuitable for real-time and accurate sensing. OHEF exhibits excellent dynamic mechanical properties, making it a promising candidate for strain sensors. Fig. 4a shows the sensitivity of OHEF-based strain sensors in different strain

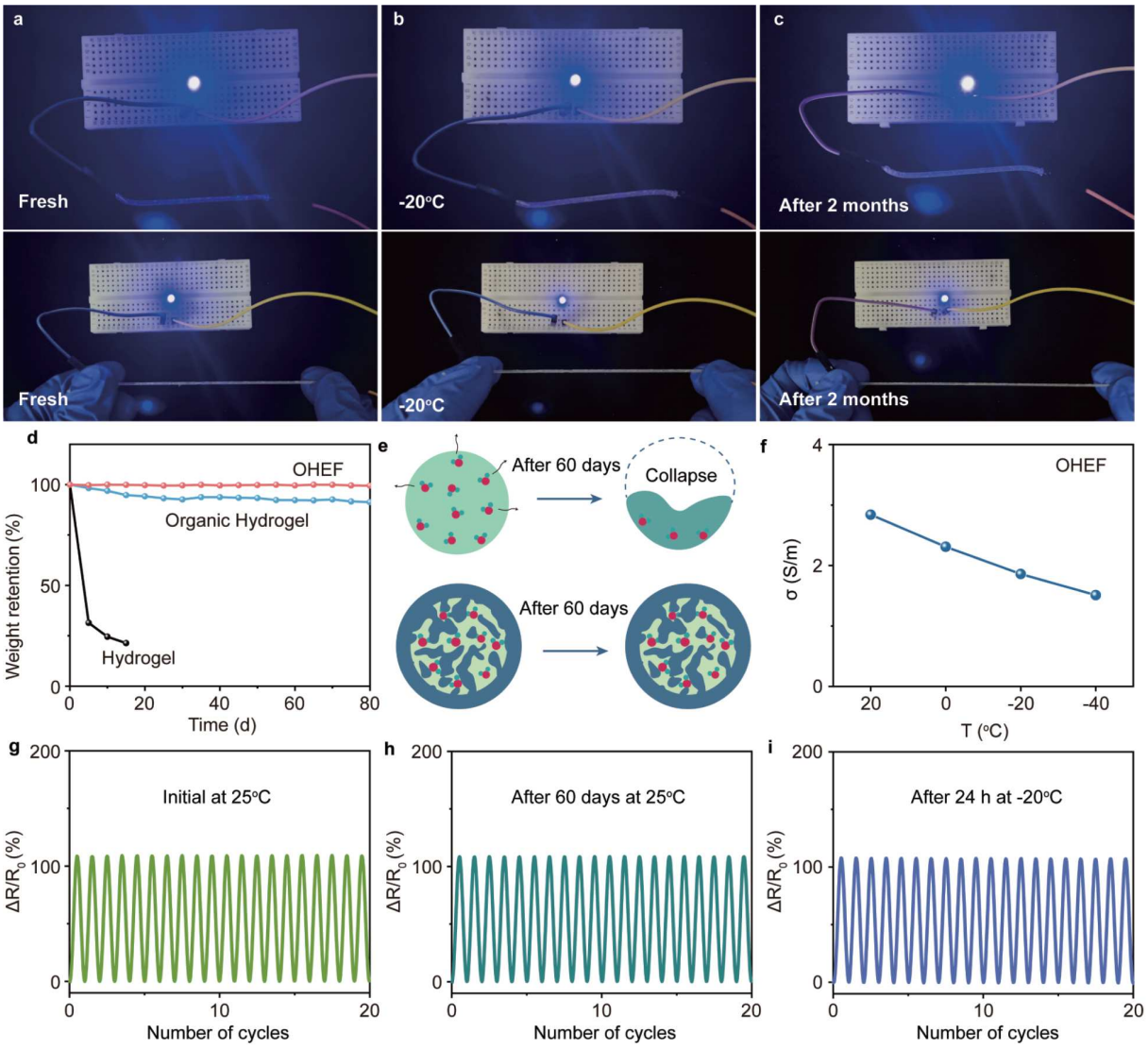

Figure 3 Anti-dehydration and anti-freezing properties of OHEF. Different OHEFs were incorporated into conductive circuits: (a) fresh OHEF, (b) OHEF at −20 °C, and (c) OHEF after 60-day placement. (d) Weight retention of hydrogel, o-hydrogel and OHEF. (e) Schematic diagram of water loss in hydrogel. (f) Electrical conductivity of OHEF at different temperatures. Cyclic tensile resistance responses of OHEF (g) in the initial state, (h) after 60 days at 25 °C, and (i) after 24 h at −20 °C.

intervals. The gauge factor (GF) values are 1.2 in the strain range of 0–200%, 2.1 in the range of 200%–400%, and 3.0 for strains exceeding 400%. OHEF shows a fast response, with response and recovery times of 114 and 113 ms, respectively (Fig. 4b). Compared with previous studies, OHEF has performance advantages due to the introduction of Ecoflex (Fig. S9). This fast-response feature is of great significance in practical applications. For instance, in human movement-monitoring scenarios, OHEF can capture the instantaneous strain changes caused by the rapid movement of human joints in real time. This ensures the timeliness and accuracy of data collection and provides a reliable basis for subsequent movement analysis and health assessment. Fig. 4c shows the current-voltage (*I-V*) linearity curve under a specific strain load, revealing the distinct ohmic behavior and static-signal stability of OHEF. Strain sensors are often used in complex scenarios, such as those with continuously changing strain and frequency. We designed two different tensile-release experiments. During the continuous-tensile-release process, the strain was gradually increased from 30% to 120%, and the resistance response of OHEF changed regularly and smoothly with the strain (Fig. 4d). Furthermore, as shown in Fig. 4e, the resistance response of the OHEF strain sensor remained relatively stable within the frequency range of 0.25–2 Hz, indicating a stable signal response over a wide frequency spectrum. The cyclic stretching of OHEF was achieved using the device shown in Fig. 4f. The circular motion of the micromotor induced the reciprocating motion of the connecting rod. The fiber was clamped between the moving rod and the fixed plate, and its resistance response was measured with a source meter. As shown in Fig. 4g, when a 70% strain was applied to the OHEF for over 10,000 tensile cycles, the resistance response remained stable and highly repeatable. This result strongly indicates that the internal structure of OHEF can remain stable and its conductivity is reliable under long-term cyclic strain, fully demonstrating the good stability and reliability of this strain sensor in practical applications. Consequently, OHEF can detect human

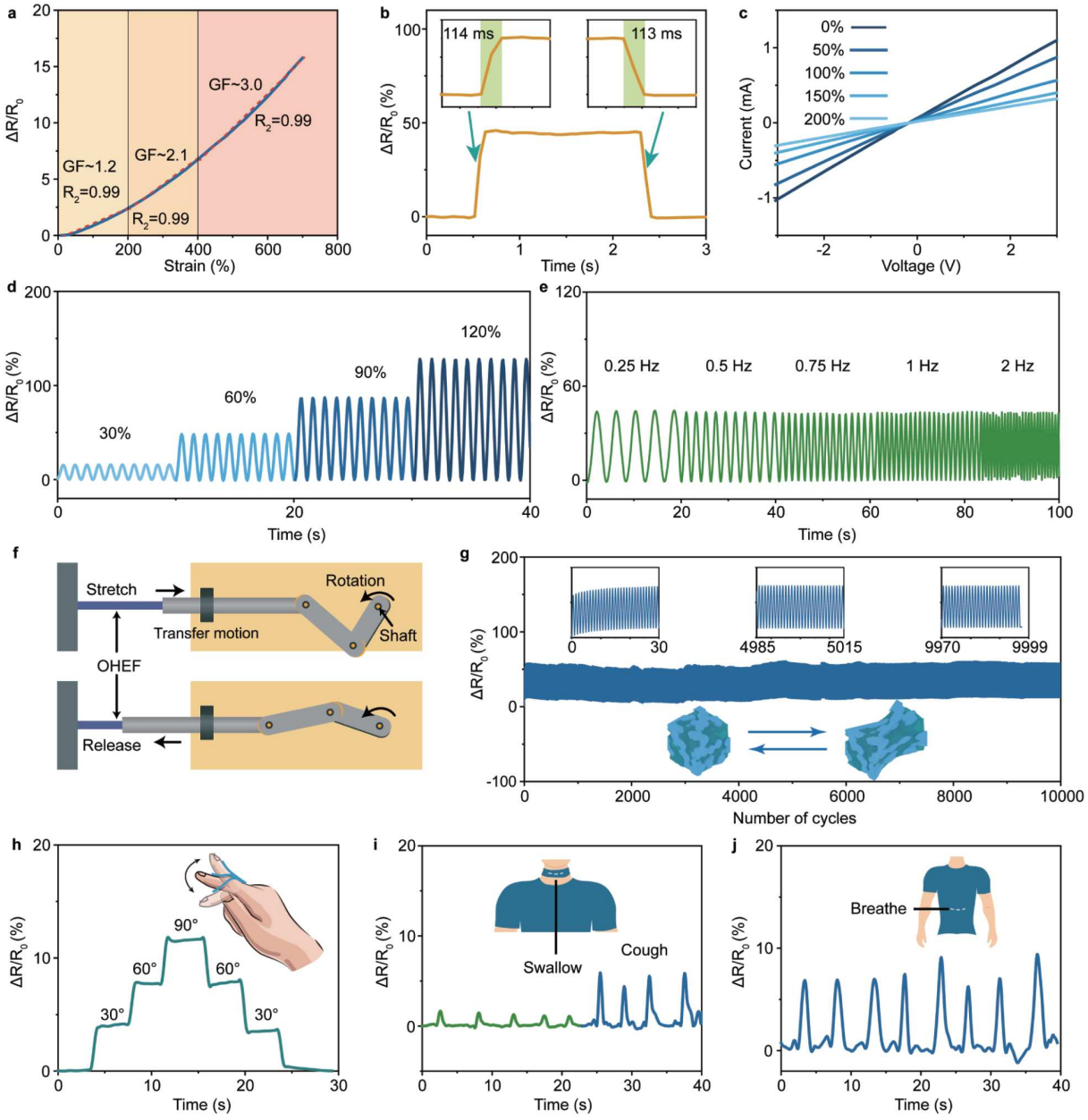

Figure 4 Response and applications of the OHEF strain sensor. (a) Strain and resistance change curves of OHEF. (b) Response time and recovery time of resistance to strain. (c) *I-V* curves of OHEF at different strains. (d) Resistance response to the same strain at different frequencies. (e) Resistance response to the same frequency at different strains. (f) Strain cycling equipment. (g) Resistance response of OHEF during 10,000 cycles at 70% strain loading and unloading. (h) Resistance response to different finger bending angles. Monitoring of (i) swallowing, coughing and (j) breathing signals.

motion and physiological signals rapidly, accurately, and sensitively. We demonstrate the integration of the OHEF strain sensor into a joint (Fig. 4h), which can sensitively detect joint movements at different angles. Furthermore, due to the high sensitivity of OHEF, it can accurately and quickly capture human physiological signals such as swallowing, coughing (Fig. 4i), and breathing (Fig. 4j). Given its extremely short response time, OHEF can detect these signals with almost no delay. This is of great significance in fields such as health monitoring, early disease diagnosis, and sports rehabilitation management. It can provide accurate data support for real-time monitoring and feedback, thus helping to improve the quality and efficiency of medical and health services.

Response of OHEF to external stimuli

The potential applications of OHEF in smart textiles were further explored. OHEF possesses a wide range of sensory capabilities and can acutely detect diverse external stimuli, such as high and low temperatures, bending, twisting, contact with sharp objects, pressure, and proximity to sharp objects. This endows smart textiles with a powerful environmental-sensing function. Therefore, these fibers can be used to fabricate smart textiles for protecting humans or robots and for promptly sensing the external environment (Fig. 5a). To demonstrate this concept, we exposed OHEF to multiple external stimuli. As shown in Fig. 5b, when OHEF was damaged, the current dropped to zero, indicating a break in the conductive path. This

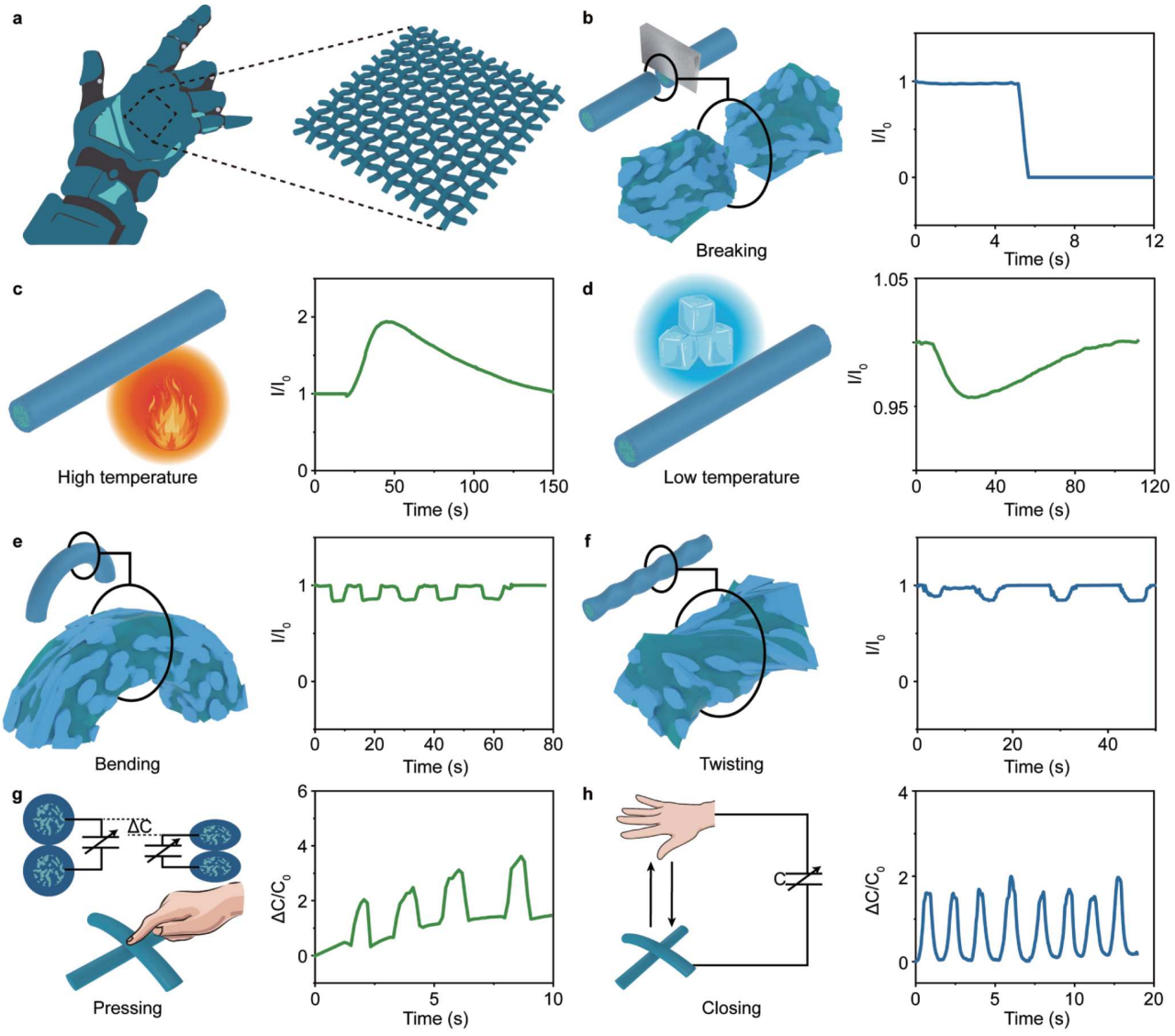

Figure 5 Responses of OHEF to external stimuli. (a) Schematic of OHEF-based smart textile. (b) Resistance response upon OHEF breakage. Resistance response signal of OHEF when exposed to (c) high and (d) low-temperature objects. Resistance response signal of OHEF when subjected to (e) bending and (f) twisting. Capacitance change when (g) pressing the OHEF and (h) approaching the OHEF.

allows for the timely detection of cuts in the smart textile. As shown in Fig. 5c, when OHEF contacted a high-temperature object (100 °C), its current increased abruptly and then returned to its initial state after about 2 min. This is because the o-hydrogel conducts electricity mainly via internal ionic transport, which is enhanced at elevated temperatures. After detaching from the high-temperature object, the electrical conductivity returns to its original level owing to the heat-resistance of Ecoflex. Conversely, as shown in Fig. 5d, when OHEF is in a low-temperature environment (−10 °C), the activity of ions is inhibited by the low temperature, and ion migration is impeded, leading to a substantial increase in its resistance. This sensitive and reversible response to high and low-temperature stimuli offers a reliable temperature-monitoring and early-warning mechanism for the application of smart textiles in extreme-temperature environments.

Regarding mechanical-deformation perception, OHEF exhibits high sensitivity to subtle deformation stimuli such as bending and twisting, as shown in Fig. 5e, f. When the fibers are twisted or bent, their internal structure changes, generating strain. Microscopically, the conductive network within the fiber is stretched or twisted, and the ion-migration paths become longer and more complex, leading to a significant increase in resistance. As shown in Fig. 5g, OHEF arranged in warp-and-weft patterns responds to pressure. Due to the low modulus of the fiber itself, when external pressure is applied, the fiber deforms, and the relative position and spacing between the warp and weft threads change, which in turn causes changes in the capacitance between the warp and weft threads. Under continuous pressure, the capacitance between the warp and weft threads drifts because of the low compression modulus of Ecoflex and the o-hydrogel and their poor post-compression resilience. It is worth noting that OHEF also has the ability for non-contact proximity sensing. A human hand repeatedly approached the fiber sensor at a vertical distance of about 20 cm (Fig. 5h), and the corresponding capacitance change was

recorded. The capacitance of the fiber sensor showed a rapid and stable change. Fig. S10 shows the non-contact position recognition of OHEF textiles achieved through this effect. In summary, OHEF can rapidly and accurately detect various external environmental stimuli through its diverse sensing-response mechanisms and precise feedback from external circuits. When OHEF is applied to e-skin or smart textiles, these excellent sensing characteristics can assist humans or robots in promptly sensing external dangers or complex stimuli and responding quickly and appropriately. From enhancing the safety and convenience of human life to promoting the autonomous operation and intelligent decision-making of robots in complex environments, OHEF has broad application prospects in the field of smart textiles. It is expected to drive a new round of innovative development in the fields of smart materials and smart applications.

OHEF-based triboelectric nanogenerator (TENG)

OHEF exhibits an electronegative surface, which enables it to function as an ideal, highly stretchable self-powered sensor based on a single-electrode-mode friction-electric mechanism (Fig. 6a) [55]. Fig. 6b illustrates the working principle of the OHEF self-powered sensor, which is based on the triboelectric effect. This study primarily demonstrates the single-electrode mode of the OHEF self-powered sensor, where the OHEF is grounded via an external load. When a moving object approaches and contacts the OHEF, due to differences in electronegativity between the two materials, their ability to restrain electrons also differs, leading to charge transfer at the interface. This results in opposite charges forming on the surface of the external material and the OHEF (Fig. 6b(i)), thereby generating a current in the load. Subsequently, when the two materials separate, the static charges on the surfaces induce charge movement within the o-hydrogel in the OHEF to balance them, bringing the OHEF to electrical neutrality (Fig. 6b(ii) and (iii)), thereby generating a current in the opposite direction within the load. When the moving object approaches the OHEF again, the entire process repeats (Fig. 6b(iv)). Therefore, continuous friction or contact will generate current in the load, which in turn can be used to detect the movement of the target material by measuring the open-circuit voltage or current. Furthermore, the ultra-high tensile properties of OHEF make it highly suitable for wearable sensing. Hence, we monitored the induced voltage of OHEF by repeatedly contacting it with five different materials:

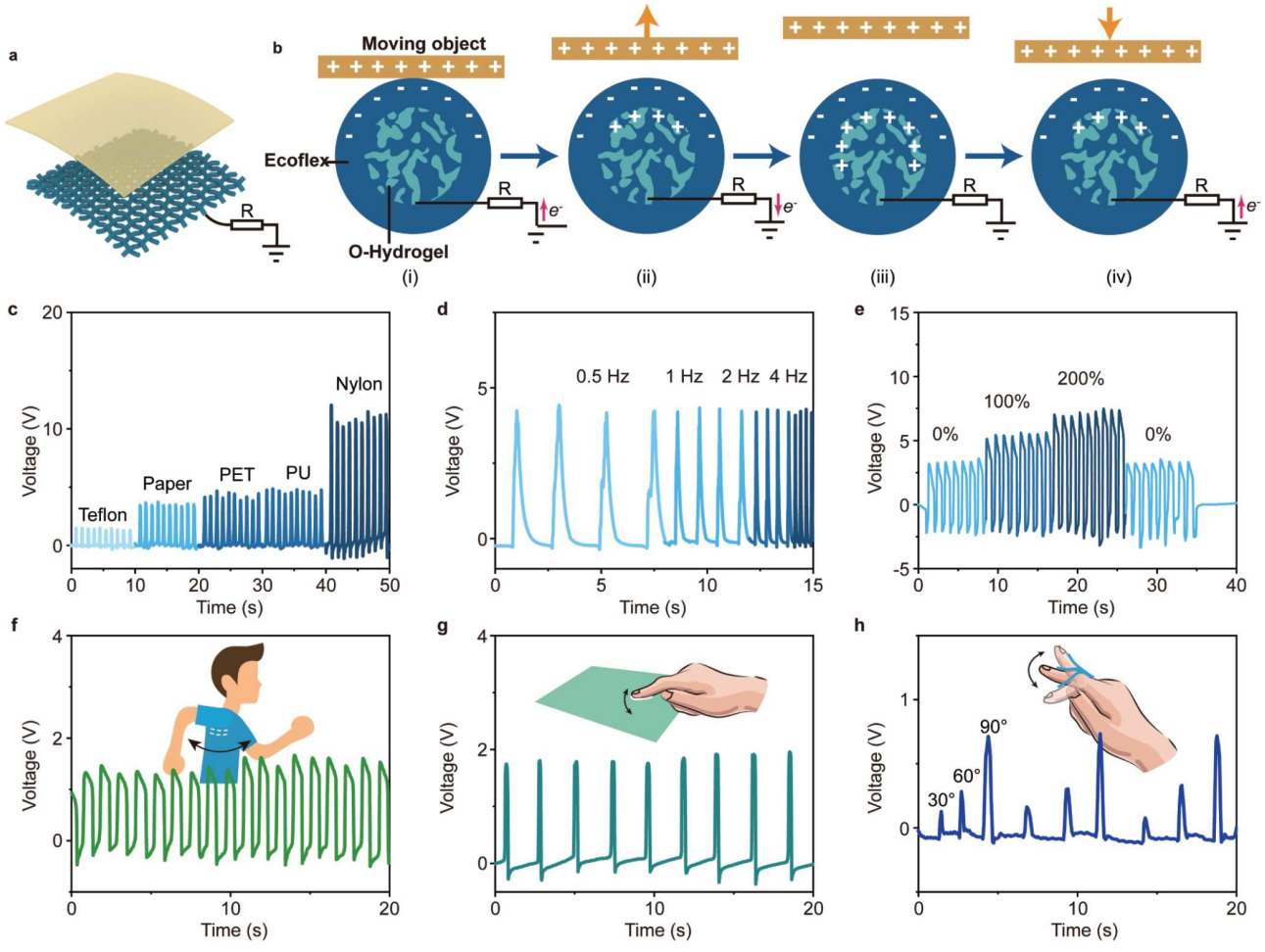

Figure 6 OHEF-based TENG. (a) Schematic of OHEF-based TENG. (b) Principles of OHEF-based TENG. (c) Voltage signals generated by OHEF-TENG when in contact with five different triboelectric materials at a motion frequency of 1 Hz. (d) Electrical signals generated at different contact frequencies. (e) Voltage signals under different OHEF strain levels. (f) OHEF-TENG self-powered sensors placed in the armpits for the stride frequency detection. (g) OHEF-TENG self-powered sensor located at the fingertips for touch signal detection. (h) OHEF-TENG self-powered sensor at the finger joints for finger flexion signal detection.

polytetrafluoroethylene (PTFE), polyethylene terephthalate (PET), polyurethane, paper, and nylon. As shown in Fig. 6c, highly reproducible voltage signals can be detected for materials with different friction-electrode properties. This indicates that OHEF-based self-powered sensors show potential for identifying material types based on differences in electron affinity. When the contact-separation frequency increased from 0.5 to 4 Hz, the induced voltage exhibited no significant change (Fig. 6d). When the fiber was stretched to higher strains, the fiber-based sensor remained operational, and an increase in voltage was observed with the increase in strain. The voltage fully recovered when the fiber was relaxed (Fig. 6e). This increase in voltage can be ascribed to the increase in contact area and the decrease in sheath thickness during stretching, which facilitate the energization process. We further assessed the self-powered sensing ability of OHEF for monitoring actual human activities. As shown in Fig. 6f, a fiber-embedded textile was placed under the armpit. The swinging-arm movement during walking caused friction between the OHEF in the textile and the garment textile, generating an induced-voltage signal that could indicate the stride frequency. Moreover, when OHEF was placed on the fingertips, its contact with external objects produced a significant voltage response (Fig. 6g). The fiber-embedded textile was placed over the knuckle. When the finger was bent, OHEF rubbed against the skin, generating a similar voltage signal. As the finger was bent to larger angles, a repeatable but increasing voltage signal was observed (Fig. 6h). This series of experimental results fully indicate the powerful sensing ability of OHEF as a self-powered wearable sensor in real-time monitoring of human movement status and capturing subtle movement changes. This lays a solid experimental foundation for its wide application in fields such as wearable medical devices, human movement analysis, and human-computer interaction, and is expected to drive technological innovation and application expansion in related fields.

CONCLUSIONS

In conclusion, in the booming era of smart wearables, this study presents an unprecedented hydrogel/elastomer composite fiber. The fiber is fabricated through the embedding of an o-hydrogel into porous Ecoflex. Due to its bicontinuous structure and the stable support and encapsulation offered by the Ecoflex skeleton, the fiber demonstrates excellent mechanical fatigue resistance. It still retains its initial mechanical stability after 10,000 tensile cycles. The embedded o-hydrogel imparts stable ionic conductivity, long-term stability, and frost resistance to the fiber. Given the excellent fatigue resistance, robustness, and conductivity of OHEF, the fiber can function as a wearable sensing textile. As a strain sensor, OHEF demonstrates a highly stable strain response. Its conductivity shows no substantial decrease after 10,000 cycles. Furthermore, the fiber simultaneously possesses multiple sensing capabilities. These capabilities allow humans or robots to respond electrically to external stimuli, such as high and low temperatures, deformation, pressure, and proximity. The OHEF developed in this study and its associated sensory textiles constitute a novel and comfortable human-machine interface. Considering its remarkable mechanical and conductive stability, it is anticipated that OHEF will be an outstanding candidate for the fabrication of smart wearable systems.

Received 2 April 2025; accepted 18 July 2025; published online 28 October 2025

1 Hasan KMF, Chen J, Chen S, *et al.* Advanced bioinspired personal thermoregulation textiles for outdoor radiative cooling. ACS Appl Mater Interfaces, 2025, 17: 3436–3447
2 Peng Y, Cui Y. Advanced textiles for personal thermal management and energy. Joule, 2020, 4: 724–742
3 Lu H, Zhang Y, Zhu M, *et al.* Intelligent perceptual textiles based on ionic-conductive and strong silk fibers. Nat Commun, 2024, 15: 3289
4 Zhou B, Yuan M, Lu H, *et al.* Large-area knittable, wash-durable, and healable smart fibers for dual-modal sensing applications. Adv Funct Mater, 2024, 34: 2404064
5 Guo Y, Li H, Li Y, *et al.* Wearable hybrid device capable of interactive perception with pressure sensing and visualization. Adv Funct Mater, 2022, 32: 2203585
6 Li Y, Qiu Z, Kan H, *et al.* A human-computer interaction strategy for an FPGA platform boosted integrated "perception-memory" system based on electronic tattoos and memristors. Adv Sci, 2024, 11: 2402582
7 Chen Y, Chen P, Zhou S, *et al.* Vinyl flanked amorphous conjugated polymer by Knoevenagel condensation of diketopyrrolopyrrole and indacenodithiophene for flexible transistor. Sci China Mater, 2025, 68: 110–116
8 Wu F, Liu Y, Zhang J, *et al.* Highly stretchable and high-mobility simiconducting nanofibrous blend films for fully stretchable organic transistors. Sci China Mater, 2023, 66: 1891–1898
9 Chen J, He T, Du Z, *et al.* Review of textile-based wearable electronics: from the structure of the multi-level hierarchy textiles. Nano Energy, 2023, 117: 108898
10 Zhao G, Zhu Y, Du T, *et al.* Multi-protection durable unidirectional water-transport fabric with personalized moisture and thermal management. Chem Eng J, 2024, 501: 157757
11 Hu X, Li TT, Shou B, *et al.* Novel personal cooling textiles revolutionizing human thermal management: principles, designs and applications. Chem Eng J, 2024, 499: 155729
12 Lin Q, Li Y, Shen G. High-performance flexible semiconductor fibres for multi-scenario communication applications. Sci China Mater, 2024, 67: 2363–2364
13 Wu Y, Mechael SS, Carmichael TB. Wearable e-textiles using a textile-centric design approach. Acc Chem Res, 2021, 54: 4051–4064
14 Weng W, Chen P, He S, *et al.* Smart electronic textiles. Angew Chem Int Ed, 2016, 55: 6140–6169
15 Ali I, Islam MR, Yin J, *et al.* Advances in smart photovoltaic textiles. ACS Nano, 2024, 18: 3871–3915
16 Wei Y, Li X, Wang Y, *et al.* Graphene-based multifunctional textile for sensing and actuating. ACS Nano, 2021, 15: 17738–17747
17 Fan W, Liu T, Wu F, *et al.* An antisweat interference and highly sensitive temperature sensor based on poly(3,4-ethylenedioxythiophene)–poly(styrenesulfonate) fiber coated with polyurethane/graphene for real-time monitoring of body temperature. ACS Nano, 2023, 17: 21073–21082
18 Zhou J, Xu X, Xin Y, *et al.* Coaxial thermoplastic elastomer-wrapped carbon nanotube fibers for deformable and wearable strain sensors. Adv Funct Mater, 2018, 28: 1705591
19 Qu X, Wu Y, Ji P, *et al.* Crack-based core-sheath fiber strain sensors with an ultralow detection limit and an ultrawide working range. ACS Appl Mater Interfaces, 2022, 14: 29167–29175
20 Chen L, Ren M, Zhou J, *et al.* Bioinspired iontronic synapse fibers for ultralow-power multiplexing neuromorphic sensorimotor textiles. Proc Natl Acad Sci USA, 2024, 121: e2407971121
21 Shi X, Zuo Y, Zhai P, *et al.* Large-area display textiles integrated with functional systems. Nature, 2021, 591: 240–245
22 Wang Y, Yuan Z, Shen G. Chipless textile electronics: human body-coupled fiber for wireless energy harvesting and signal transmission. Sci China Mater, 2024, 67: 2367–2368
23 Zou J, Feng G, Wu J, *et al.* An integrated electronic textile system capable of displaying full-color images and videos. Sci China Mater, 2024, 67: 3021–3028
24 Lu C, Jiang H, Cheng X, *et al.* High-performance fibre battery with

polymer gel electrolyte. Nature, 2024, 629: 86–91
25 Huang X, Wang C, Li C, *et al.* Braided fiber current collectors for high-energy-density fiber lithium-ion batteries. Angew Chem, 2023, 135: e202303616
26 Wang L, Zhang M, Yang B, *et al.* Lightweight, robust, conductive composite fibers based on MXene@aramid nanofibers as sensors for smart fabrics. ACS Appl Mater Interfaces, 2021, 13: 41933–41945
27 Wang Q, Zhang H, Liu J, *et al.* Multifunctional and water-resistant MXene-decorated polyester textiles with outstanding electromagnetic interference shielding and Joule heating performances. Adv Funct Mater, 2019, 29: 1806819
28 Mei L, Sun M, Yang R, *et al.* Metallic 1T/1T′ phase TMD nanosheets with enhanced chemisorption sites for ultrahigh-efficiency lead removal. Nat Commun, 2024, 15: 7770
29 Yang R, Fan Y, Mei L, *et al.* Synthesis of atomically thin sheets by the intercalation-based exfoliation of layered materials. Nat Synth, 2023, 2: 101–118
30 Mei L, Gao Z, Yang R, *et al.* Phase-switchable preparation of solution-processable WS_2 mono- or bilayers. Nat Synth, 2025, 4: 303–313
31 Sun F, Tian M, Sun X, *et al.* Stretchable conductive fibers of ultrahigh tensile strain and stable conductance enabled by a worm-shaped graphene microlayer. Nano Lett, 2019, 19: 6592–6599
32 Luo X, Weng W, Liang Y, *et al.* Multifunctional fabrics of carbon nanotube fibers. J Mater Chem A, 2019, 7: 8790–8797
33 Wei D, Lv S, Zuo J, *et al.* Engineering versatile bi-network ionic conductive hydrogels wearable sensors via on demand graft modification for real-time human movement monitoring. Chem Eng J, 2024, 496: 154176
34 Li Z, Lu J, Ji T, *et al.* Self-healing hydrogel bioelectronics. Adv Mater, 2024, 36: 2306350
35 Zhang M, Yu R, Tao X, *et al.* Mechanically robust and highly conductive ionogels for soft ionotronics. Adv Funct Mater, 2023, 33: 2208083
36 Xue C, Zhao Y, Liao Y, *et al.* Bioinspired super-robust conductive hydrogels for machine learning-assisted tactile perception system. Adv Mater, 2025, 37: 2416275
37 Wang G, Jing X, Niu B, *et al.* Ultrasensitive conductive hydrogels conferred by nanoscale synergistic effect. Sci China Mater, 2025, 68: 226–235
38 Zhan W, Zhang H, Lyu X, *et al.* An ultra-tough and super-stretchable ionogel with multi functions towards flexible iontronics. Sci China Mater, 2023, 66: 1539–1550
39 Ran X, Shi Z, Zhang A, *et al.* Efficient passive cooling for photovoltaic cells via self-hygroscopic polyvinyl alcohol/graphene films. SmartMat, 2025, 6: e70015
40 Guo Y, Yin F, Li Y, *et al.* Incorporating wireless strategies to wearable devices enabled by a photocurable hydrogel for monitoring pressure information. Adv Mater, 2023, 35: 2300855
41 Xue X, Hu Y, Wang S, *et al.* Fabrication of physical and chemical crosslinked hydrogels for bone tissue engineering. Bioactive Mater, 2022, 12: 327–339
42 Liu S, Luan Z, Wang T, *et al.* Endoscopy deliverable and mushroom-cap-inspired hyperboloid-shaped drug-laden bioadhesive hydrogel for stomach perforation repair. ACS Nano, 2023, 17: 111–126
43 Yao M, Wei Z, Li J, *et al.* Microgel reinforced zwitterionic hydrogel coating for blood-contacting biomedical devices. Nat Commun, 2022, 13: 5339
44 Ding X, Yu Y, Shang L, *et al.* Histidine-triggered GO hybrid hydrogels for microfluidic 3D printing. ACS Nano, 2022, 16: 19533–19542
45 Tang Y, Lu C, Xiong R. Biomimetic mechanically robust chiroptical hydrogel enabled by hierarchical bouligand structure engineering. ACS Nano, 2024, 18: 14629–14639
46 Lu Y, Yang G, Wang S, *et al.* Stretchable graphene–hydrogel interfaces for wearable and implantable bioelectronics. Nat Electron, 2023, 7: 51–65
47 Qu J, Yuan Q, Li Z, *et al.* All-in-one strain-triboelectric sensors based on environment-friendly ionic hydrogel for wearable sensing and underwater soft robotic grasping. Nano Energy, 2023, 111: 108387
48 Guan QF, Yang HB, Han ZM, *et al.* Sustainable cellulose-nanofiber-based hydrogels. ACS Nano, 2021, 15: 7889–7898
49 Shi H, Huo H, Yang H, *et al.* Cellulose-based dual-network conductive hydrogel with exceptional adhesion. Adv Funct Mater, 2024, 34: 2408560
50 Yao X, Zhang S, Wei N, *et al.* Cellulose-based conductive hydrogels for emerging intelligent sensors. Adv Fiber Mater, 2024, 6: 1256–1305
51 Pan X, Li J, Ma N, *et al.* Bacterial cellulose hydrogel for sensors. Chem Eng J, 2023, 461: 142062
52 Wang Z, Zhu M, Li J, *et al.* Nanocellulose based hydrogel for flexible sensors: current progress and future perspective. Nano Energy, 2024, 129: 109974
53 Li S, Xu J, Mu Y, *et al.* Fatigue-resistant and hysteresis-free composite fibers with a heterogeneous hierarchical structure. Adv Fiber Mater, 2023, 5: 1643–1656
54 Song J, Chen S, Sun L, *et al.* Mechanically and electronically robust transparent organohydrogel fibers. Adv Mater, 2020, 32: 1906994
55 Luo X, Zhu L, Wang Y, *et al.* A flexible multifunctional triboelectric nanogenerator based on MXene/PVA hydrogel. Adv Funct Mater, 2021, 31: 2104928

Acknowledgement This work was supported by the National Natural Science Foundation of China (12234005 and T2321002), the Natural Science Foundation of Chongqing (2022NSCQ-MSX2366), and the Open Research Fund of Key Laboratory of MEMS of Ministry of Education, Southeast University.

Author contributions Shen J and Sun L conceived the idea and designed the experiments; Shen J, Li C, and Hou S analyzed the data; Yin K and Sun L provided experimental guidance; Shen J, Feng T and Bi H wrote the initial draft of the manuscript, which was then revised by other coauthors. All of the authors have approved the final version of the manuscript.

Conflict of interest The authors declare that they have no conflict of interest.

Supplementary information Supplementary materials are available in the online version of the paper.

Jiaxin Shen is currently a PhD student in the Nano-Pico Center of Southeast University, supervised by Prof. Litao Sun. His major research interests are micro-nano regulation, structural design and application research of wearable flexible energy and sensing systems.

Hengchang Bi received his PhD degree in Engineering from Southeast University in 2016 (supervisor: Prof. Litao Sun) and is currently a researcher at East China Normal University. His main research interests include artificial intelligence, flexible smart sensor systems and wearable devices, semiconductor materials and devices, MEMS micro- and nanoelectromechanical systems and devices, and integrated circuit design.

Litao Sun received his PhD degree from Shanghai Institute of Applied Physics, Chinese Academy of Sciences in 2005. He worked as a research fellow at the University of Mainz from 2005 to 2008, and a visiting professor at the University of Strasbourg from 2009 to 2010. He joined Southeast University as a distinguished professor in 2008. His work focuses on cutting-edge fundamental research and applications of nanomaterials in micro-nano systems, renewable energy and environmental protection.

具有多传感功能的高强度抗疲劳有机水凝胶复合弹性纤维

申佳欣[1], 冯涛[1], 李陈[1], 后士胜[1], 尹奎波[1], 毕恒昌[2,3*], 孙立涛[1*]

摘要 将水凝胶转化为纤维结构并集成到纺织品中，在智能可穿戴领域极具发展前景. 当水凝胶遭遇变形时，其内部低能无定形聚合物链会发生断裂，这直接导致了水凝胶的疲劳和滞后问题. 本研究将Ecoflex弹性体骨架集成到有机水凝胶中，成功制备出一种高强度抗疲劳的有机水凝胶/Ecoflex纤维(OHEF). OHEF在200%应变下进行10,000次加载和卸载循环，其机械性能无明显降低. 此外，OHEF具备出色的抗脱水和耐冷冻性能. 基于OHEF的应变传感器，具有高灵敏度(GF为3.0)、快速响应(0.14 s)/恢复时间(0.13 s)和优异的可重复性(70%应变下10,000次循环). OHEF的智能纺织品可以检测各种外部刺激，包括各种形变、温度、靠近和压力，并能进行基于摩擦电的自驱动传感. OHEF的成功开发凸显了水凝胶在可穿戴电子纺织品中的巨大潜力.